A Fast Rotating-Mirror Sounder for Dynamic Millimeter-Wave Channel Characterization

Al-Ameri, Ali; Sanchez, Juan; Tufvesson, Fredrik; Cai, Xuesong

Published in:
Proc. IEEE 100th Veh. Technol. Conf. (VTC2024-Fall)

2024

Document Version:
Peer reviewed version (aka post-print)

A Fast Rotating-Mirror Sounder for Dynamic Millimeter-Wave Channel Characterization

Ali Al-Ameri, Juan Sanchez, Fredrik Tufvesson, and Xuesong Cai
Department of Electrical and Information Technology, *Lund University*, Lund, Sweden
{ali.al-ameri, juan.sanchez, fredrik.tufvesson, xuesong.cai}@eit.lth.se

***Abstract*—A deep understanding of double-directional wireless channels is imperative for wireless system design. This necessitates the development of precise channel models through channel sounding. Given the dynamic nature of wireless channels, a short measurement time is highly desirable. In this paper, we present and validate a dual-polarized millimeter-wave channel sounder that uses a rotating mirror mechanism. This enables quick sweep of the azimuthal plane to capture spatial channel characteristics at 27.5-28.5 GHz in less than a second. This is radically faster than conventional virtual-array channel sounders. Following a detailed discussion of the sounder implementation and the rotating mirror concept, we present an indoor verification measurement scenario. The results demonstrate several discernible propagation paths with parameters that agree with the actual geometry of the indoor measurement environment.**

***Index Terms*—Channel sounder design, dynamic channels, millimeter-wave, propagation measurements, and parameter estimation.**

I. Introduction

In recent years, there has been a notable upsurge in the interest in utilizing the spectrum within the millimeter-wave (mmWave) and sub-terahertz frequency bands. This trend is mainly due to the abundance of available bandwidth at these frequencies for communications, sensing, and localization [3]. The use of these frequencies is often combined with the use of a large number of antennas through the adoption of massive multiple-input multiple-output (MIMO) systems. This is done primarily to mitigate challenges such as increased path loss and to achieve higher bandwidth efficiency to meet the ever-increasing data rate demands of today's society [4], [5].

To design and evaluate such MIMO systems, a comprehensive understanding of double-directional mmWave wireless channels is crucial. To this end, measurement-based channel models through channel sounding are irreplaceable in understanding the complex propagation mechanisms involved. This is usually done in three main steps. First, the channel is measured using a channel sounder. Next, high-resolution parameter estimation algorithms are used to extract channel parameters. Finally, these extracted parameters are used to model the channel behavior in domains such as power, space, delay, and Doppler frequency.

Developing precise channel models requires the development of carefully designed channel sounders to capture accurate channel data. Generally, a channel sounder operates as a device where the transmitter (Tx) emits a predefined waveform known to the receiver (Rx). Following propagation through the channel, the signal is received by the Rx, which deconvolves the transmitted waveform from the received signal, yielding solely the channel impulse response (CIR).

Different channel sounder architectures can be utilized to measure dynamic double-directional channels. One such architecture, the so-called real array channel sounder, measures the MIMO channel using several radio frequency (RF) chains, one for each antenna element [6]–[8]. Although this method is fast and thus advantageous for capturing dynamic channels, it is costly due to expensive RF components. Additionally, real-array sounders are difficult to calibrate because of the presence of a large (possibly massive) number of RF chains. A common method in the literature is the use of virtual-arrays [9]–[11]. This approach captures the spatial characteristics of the channel by mechanically moving the Tx and Rx antennas to different orientations/positions and measuring the channel characteristics. Although this method is simple and cost-effective, the main drawback of such an approach is that a measurement can take several tens of minutes, making it an unviable option for dynamic channel measurements. Another sounding technique is the use of switched arrays [12], where a single RF chain transmits/receives through different antenna elements in a predefined sequence through an RF switch [13]. This approach strikes a balance between cost, calibration complexity, and measurement speed, as it uses a single RF chain. Furthermore, this method is capable of capturing MIMO snapshots containing all antenna pair combinations in a very short measurement time due to RF switches with switching rates in the order of a few microseconds. However, the lack of reliable, fast, and low-attenuation RF switches at higher frequencies (e.g. sub-terahertz bands) hinders the reconfigurability of switched array sounders.

To this end, the contribution of this paper lies in the design, implementation, and performance verification of a mmWave

This work has been funded by the Swedish Research Council (Grant No. 2022-04691), the Horizon Europe Framework Programme under the Marie Skłodowska-Curie grant agreement No. 101059091, the Horizon 2020 EU Framework Programme under Grant Agreement No. 861222, the Royal Physiographic Society of Lund, the Strategic Research Area Excellence Center at Linköping–Lund in Information Technology (ELLIIT), and Ericsson. The authors acknowledge the inspiring discussions with Andreas F. Molisch and Christoph Mecklenbräuker. They were the first to mention the possibility of using rotating mirrors for channel sounding [1], and their independent realization at 60 GHz can be found in [2]. The authors also acknowledge the contributions of Martin Nilsson and Meifang Zhu to the sounder development.

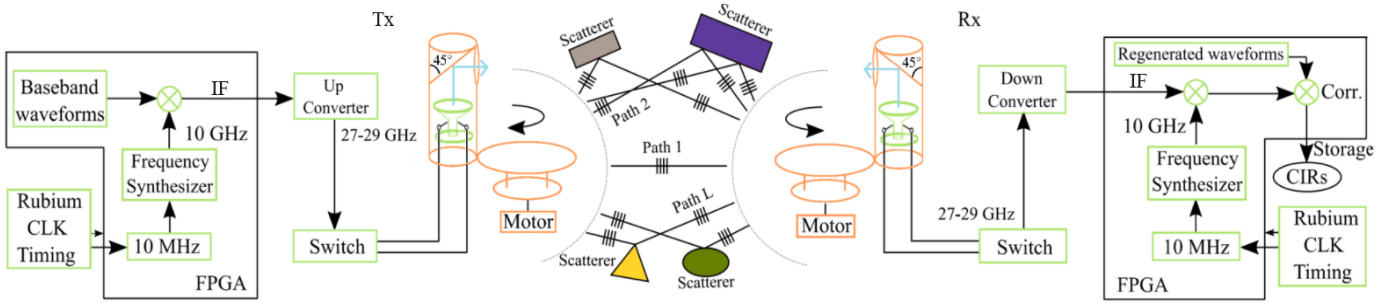

Fig. 1: Block diagram showing the various sounder components at both the Tx and Rx.

channel sounder using a fast rotating mirror technique. This approach uses one mirror at the Tx side and another at the Rx side. The Tx mirror reflects the signal emitted by the Tx horn antenna toward the channel in a single elevation cut, while the mirror at the Rx side reflects the incoming signals towards the Rx horn antenna. This mirror technique allows us to have the simplicity and cost-effectiveness of a virtual-array while achieving measurement speeds similar to that of a switched array. Furthermore, it allows for a high degree of reconfigurability, as it is possible to use this mirror technique at much higher frequencies than those achievable by switched arrays. Besides [2], a channel sounder that utilizes mirrors has been presented in [14]. However, it is important to note that the latter is not capable of dynamic channel measurements due to its lengthy measurement duration, which is on the order of several minutes.

The remainder of the paper is structured as follows. Sect. II presents the design and implementation aspects of the sounder. In Sect. III, the verification measurement scenario is presented and the results are shown. Finally, in Sect. IV, conclusions are drawn and remarks about future work are outlined.

II. Channel Sounder Design and Practical Considerations

This section provides a detailed step-by-step discussion of different design aspects and practical considerations for the sounder. For clarity, we divide this section into several sub-sections. We start by looking at the overall sounder structure.

A. Channel sounder setup and implementation

Our sounder is a time-domain correlation-based channel sounder. It operates in the mmWave band and can capture channel information in both vertical (V) and horizontal (H) polarizations using dual polarized narrow beamwidth horn antennas.

The implementation of the sounder can be seen in Fig. 1. First, the operation of the sounder begins with the baseband waveform generation (details about the waveform follow in the next subsection). The generated waveform is converted to an analog baseband signal through a digital-to-analog converter (D/A). The baseband signal is then mixed to an intermediate frequency (IF) signal centered at 10 GHz through a frequency synthesizer with a 10 MHz clock reference (CLK) sourced from a rubidium clock. After the IF stage, the signal is upconverted to the desired 28 GHz mmWave RF signal. The signal then passes through the switching circuit that is connected to the V- and H- ports of a horn antenna placed underneath the spinning mirror. The antenna transmits the signal towards the mirror, reflecting it towards the channel to capture the spatial characteristics in the azimuth domain.

At the Rx, the received signal hits the mirror, being reflected towards the Rx horn antenna, which feeds the RF signal to the switching circuit. The signal is then downconverted back to IF and further mixed to baseband. The baseband signal is correlated with the known transmitted waveform to extract the CIR which is stored for later postprocessing.

B. Waveform Design

In a similar fashion to [12], we exploit the so-called Zadoff-Chu (ZC) sequence. We do this because of its advantageous correlation properties in both time and frequency domains, making it appropriate to use as our baseband sounding waveform. We choose our ZC waveform parameters to achieve a high delay resolution and a wide range of maximum observable multipath component (MPC) delays. We choose a sequence length of 2047 samples. Combined with a transmission rate of 768 MHz, this parameter configuration gives a delay resolution of 0.4 m and a maximum observable delay of 2.7 μs which corresponds to a propagation distance of around 800 m.

To achieve increased robustness, the same ZC sequence may be transmitted several times and averaged at the receiver for one CIR. In our implementation, the average factor is seven. In addition, we append two guard sequences before and after the seven ZC sequences to protect against clock reference drifts. A margin sequence is also included to account for the MPC delays. These sequences, along with guard periods for the switch settling time, result in a CIR capture time of around 27 μs. It is important to note that this transmission structure is highly flexible. For example, we could drastically reduce the CIR capture time by reducing the number of averaged sequences.

C. The Rotating Mirror

A rapidly rotating mirror capable of reflecting RF signals in the mmWave range facilitates the interaction between the

wireless channel and the transmitting/receiving horn antennas. All of the wired components (including antennas) are stationary, while the only moving parts are the mirrors. The mirror structure enables very fast rotations without entangling or damaging the fragile feeding wires to the antennas. This allows for fast channel measurements, a feature yet to be achieved with standard virtual-array sounders.

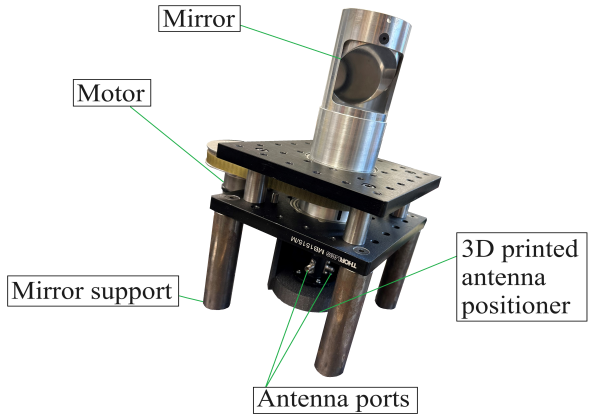

Fig. 2: Tx mirror setup.

The mirror construction at the Tx side can be seen in Fig. 2. Note that the horn antenna is placed directly below the metallic mirror housing, held by a 3D-printed positioner designed to ensure that the antenna beam hits the center of the mirror. The mirror is in turn placed at a 45° angle relative to the horizontal axis to measure a single elevation cut.

Determining the rotation speeds for our mirrors involves several considerations. Firstly, to capture a snapshot containing all combinations of the Tx and Rx mirror orientations, the two sides have to rotate at different speeds. Secondly, the rotation speeds determine the time it takes to capture a snapshot. For a fixed sampling rate (time to capture one CIR), there is a trade-off between minimizing the snapshot duration and maintaining a high angular resolution. Faster rotation reduces the angular sample density, leading to a reduced angular resolution. However, slower rotation does not ensure a higher angular resolution beyond a certain point, since the ultimate limit for spatial resolution is set by the half-power beam width (HPBW) of our horn antennas. In our setup, we use horn antennas with HPBW (half-power beam width) of 16° and 13° for the Tx and Rx respectively. Since the sampling period is 27 μs, it takes 54 μs to sample in both polarizations. We let the Tx rotate at 2420 rpm = 40.33 Hz and the Rx rotate at 2500 rpm = 41.67 Hz. With these rotation speeds and sampling rates, we achieve inter-sample angle intervals at the Tx and Rx that are smaller than their respective HPBWs. Due to the 80-rpm offset in the rotation speeds, each time the Rx completes a full rotation, the Tx lags $360 \cdot \left(1 - \frac{40.33}{41.67}\right) = 11.52°$ behind. This means that the Tx lags a full rotation behind the Rx after $\frac{360}{11.52} = 31.25$ Rx rotations, which takes the Rx $\frac{31.25}{41.67} = 0.75$ s to complete. After this, the Tx and Rx pattern of angle orientations repeats, establishing our snapshot duration of 0.75 s. It is possible to achieve even faster measurements without degrading the angular resolution due to our sounder having the ability to capture the CIRs at such a high rate. We can make our sounder sample at an even higher rate by reconfiguring the sounding waveform as mentioned in the previous subsection.

D. Synchronization Aspects

In order to post-process the measurement data, it is crucial to know the mirror positions at the Tx and Rx sides when different samples are collected. For this, each mirror is equipped with an optical sensor that is triggered once per rotation when a machined hole slot on the cylindrical mirror housing passes by the sensor. The optical sensors are combined with Hall effect sensors on both sides, which provide an additional seven pulses per rotation. Each pulse gives us the mirror orientation at its corresponding timestamp, and the continuous position of the mirror can be interpolated using this information. Notice that sensor pulses are recorded on two separate Tx and Rx Field-Programmable Gate Arrays (FPGAs), meaning that the pulse timestamps are relative to the individual FPGAs. Therefore, a synchronization mechanism between the two FPGAs is necessary to determine the positions of the mirrors relative to each other.

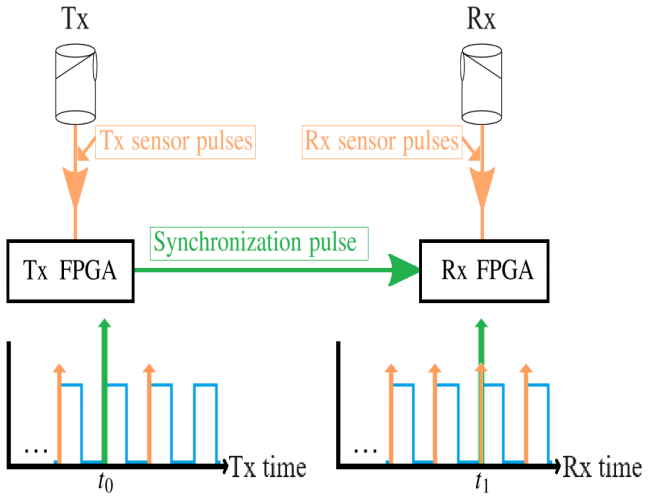

Fig. 3: Synchronization procedure.

Our method for achieving such synchronization is illustrated in Fig. 3. The FPGA tick rates are depicted in blue, the sensor pulses are in orange, and the synchronization pulse is in green. Before the measurement begins, the Tx transmits a pulse (either through a wire or wirelessly) to the Rx and records this pulse generation time t_0 relative to the Tx FPGA. This pulse is then received by the Rx at time t_1 relative to the Rx FPGA. The time difference between the two sides is

obtained as $\Delta = t_1 - t_0$, and finally stored for compensation during post-processing.

E. Channel Sounder Parameters

We conclude this section by summarizing the parameters of our channel sounder in Table 1, which shows the reconfigurability of our sounder.

Parameter	Value
Sounder type	Correlation based
Center frequency	28 GHz
Bandwidth*	up to 2 GHz
Tx rotation speed*	2500 rpm
Rx rotation speed*	2420 rpm
Tx horn antenna 3 dB beamwidth	16°
Rx horn antenna 3 dB beamwidth	13°
Duration between two samples*	27 μs
Snapshot duration*	0.75 s

TABLE I: Channel sounder parameters. Reconfigurable parameters are marked with *.

III. Measurement Results

In this section, we present our verification measurement scenario. After that, we discuss our measurement results, comparing them with the geometry of the measurement environment.

A. Measurement Scenario

The measurements were performed in an indoor laboratory environment at the Department of Electrical and Information Technology, Lund University. The measurement environment is illustrated in Fig. 4, where we can observe the positions of the Tx (marked in red) and Rx (marked in green) relative to each other and to the four walls "A", "B", "C" and "D". Furthermore, two reflectors "R1" and "R2" were placed in the measurement environment. R1 was placed facing the Tx past the Rx when looking from the Tx perspective, while R2 is positioned close to the Rx at an angle.

A real-life image of the measurement environment is provided in Fig. 5, showing the Tx and Rx mirror setups as well as the reflectors used. This figure also displays walls, ceiling, tables and numerous equipment present in the lab.

For the verification measurement, the sounder parameters were set as in Table I. Although the effective measurement bandwidth is configured to 768 MHz and the measurement duration was set to 0.96 s. This extra time margin is there to ensure that the time it takes to capture all Tx and Rx orientations (0.75 s) falls comfortably within the measurement time, to protect against the risk of rotational instability. This margin does not have a negative consequence on our results given the static measurement environment.

B. Results

Fig. 6 presents the delay Tx-azimuth and delay Rx-azimuth power spectra. Several propagation paths are discernible and marked in the figure. We can recognize the strongest path at Tx-azimuth and Rx-azimuth angles of around 270° and 90°,

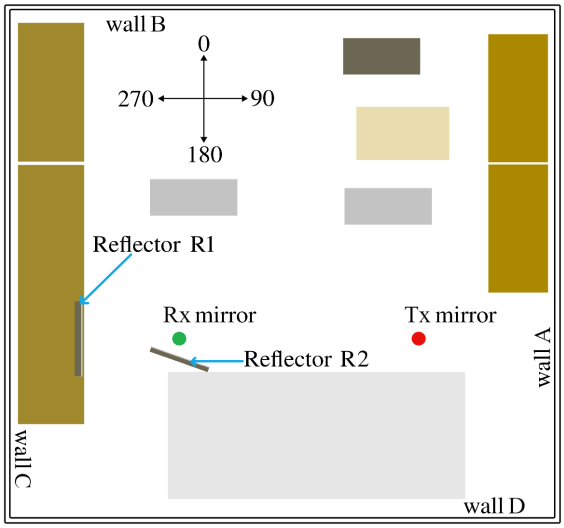

Fig. 4: Measurement environment.

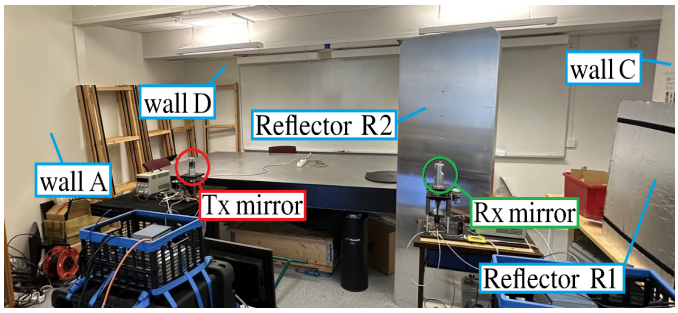

Fig. 5: Actual measurement environment.

respectively. This combination of angles represents the Tx and Rx mirrors facing each other, and the associated multipath component corresponds to the Line-Of-Sight (LOS) path. We can also see two Non Line-Of-Sight (NLOS) paths, labeled "NLOS 1" and "NLOS 2". Noting that NLOS 1 occurs at Tx-azimuth of 254° and Rx-azimuth of 155°, we can say with a high degree of confidence that this path is the reflection from reflector R2. Since NLOS 2 occurs at an azimuth angle close to 270° at both sides, it can be concluded that this path is a reflection induced by R1. In addition, the delay differences of 0.4 m between LOS and NLOS 1, and 1.9 m between LOS and NLOS 2, are consistent with the relative placement of the two reflector panels with respect to the two mirrors.

Fig. 7 illustrates the power of the received signal as a function of Rx-azimuth and Tx-azimuth integrated over the entire range of delays. Here, we once again note the LOS path along with NLOS 1 and NLOS 2. Furthermore, we notice several other marked paths "NLOS 3", "NLOS 4", and "NLOS 5". NLOS 3 peaks at Tx-azimuth of 92° and Rx-azimuth of 268°, indicating a path that experienced a double reflection, once on wall A and then again at R1 before reaching the Rx. Similarly, NLOS 4 reflects twice, once at wall A and then again at R2. Finally, NLOS 5 is the wall reflection from wall

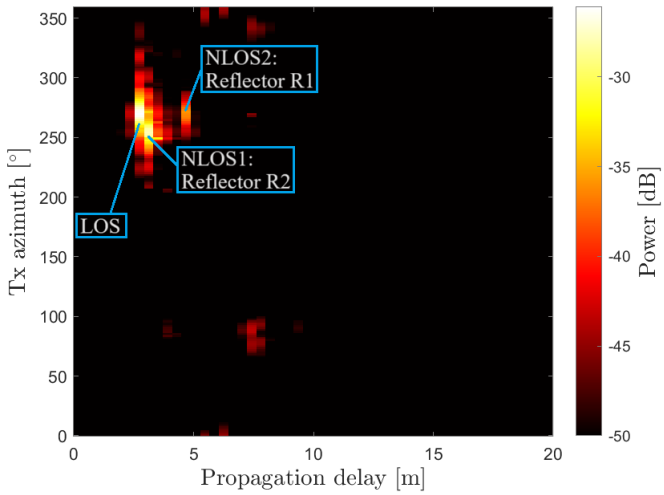

(a)

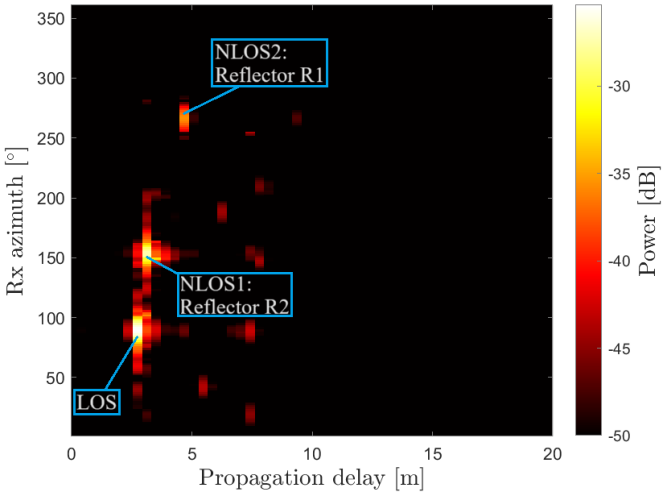

(b)

Fig. 6: Received signal power spectra. (a) Delay Tx-azimuth domain. (b) Delay Rx-azimuth domain.

A.

To summarize, we have successfully identified several paths in Fig. 6 and Fig. 7. These paths are consistent with the real measurement environment geometry and verify the proposed sounder. It is worth noting that there are more paths than the ones we identified, indicating the richness of multipath components in the lab.

IV. Conclusions

We presented and verified a novel highly reconfigurable mmWave channel sounder that uses rapidly rotating mirrors to capture spatial channel characteristics in less than a second. We discussed several design and implementation aspects. The functionality of the sounder was verified with indoor measurements. Future work will utilize this sounder for characterizing mmWave channels in different scenarios and extend its operation frequency to higher frequencies such as the sub-terahertz band.

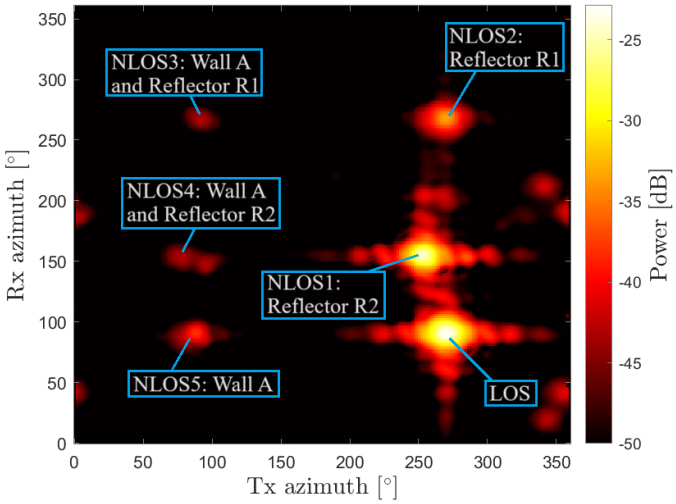

Fig. 7: Received signal power spectrum over Rx-azimuth and Tx-azimuth angles.

References

[1] A. Molisch *et al.*, "Spinning directional antenna in centimeter and millimeter wave bands," no. WO 2022155493 A1 Patent, 2022.

[2] H. Hammoud *et al.*, "A novel low-cost channel sounder for double-directionally resolved measurements in the mmwave band," in *IEEE International Conference on Communications (ICC)*, 2024.

[3] X. Cai, X. Cheng, and F. Tufvesson, "Toward 6G with terahertz communications: Understanding the propagation channels," *IEEE Communications Magazine*, vol. 62, no. 2, pp. 32–38, 2024.

[4] C. Han *et al.*, "Terahertz wireless channels: A holistic survey on measurement, modeling, and analysis," *IEEE Communications Surveys & Tutorials*, vol. 24, no. 3, pp. 1670–1707, 2022.

[5] X. Wang *et al.*, "Millimeter wave communication: A comprehensive survey," *IEEE Communications Surveys & Tutorials*, vol. 20, no. 3, pp. 1616–1653, 2018.

[6] P. Laly *et al.*, "Flexible real-time MIMO channel sounder for multidimensional polarimetric parameter estimation," in *IEEE Conference on Antenna Measurements & Applications (CAMA)*, 2015.

[7] X. Cai *et al.*, "Empirical low-altitude air-to-ground spatial channel characterization for cellular networks connectivity," *IEEE Journal on Selected Areas in Communications*, vol. 39, no. 10, pp. 2975–2991, 2021.

[8] D. Stanko *et al.*, "Enable SDRs for real-time MIMO channel sounding featuring parallel coherent Rx channels," in *IEEE 95th Vehicular Technology Conference (VTC2022-Spring)*, 2022.

[9] W. Fu, J. Hu, and S. Zhang, "Frequency-domain measurement of 60 GHz indoor channels: A measurement setup, literature data, and analysis," *IEEE Instrumentation & Measurement Magazine*, vol. 16, no. 2, pp. 34–40, 2013.

[10] A. W. Mbugua *et al.*, "Phase-compensated optical fiber-based ultrawideband channel sounder," *IEEE Transactions on Microwave Theory and Techniques*, vol. 68, no. 2, pp. 636–647, 2020.

[11] C. Gustafson *et al.*, "Directional analysis of measured 60 GHz indoor radio channels using SAGE," in *IEEE 73rd Vehicular Technology Conference (VTC Spring)*, 2011.

[12] X. Cai *et al.*, "A switched array sounder for dynamic millimeter-wave channel characterization: Design, implementation and measurements," *IEEE Transactions on Antennas and Propagation (early access)*, 2024.

[13] A. Al-Ameri *et al.*, "A hybrid antenna switching scheme for dynamic channel sounding," in *IEEE 97th Vehicular Technology Conference (VTC2023-Spring)*, 2023.

[14] A. Hirata, "Measurement of 300 GHz band radio propagation characteristics in the vicinity of human body using terahertz hemispheric scanner," in *IEEE International Symposium on Antennas and Propagation and USNC-URSI Radio Science Meeting (USNC-URSI)*, 2023, pp. 1221–1222.